Planetary and Space Science 57 (2009) 744–750

Contents lists available at ScienceDirect

Planetary and Space Science

journal homepage: www.elsevier.com/locate/pss

X-ray fluorescence observations of the moon by SMART-1/D-CIXS and the first detection of Ti Kα from the lunar surface

B.M. Swinyard [a,*], K.H. Joy [a,b,c], B.J. Kellett [a], I.A. Crawford [b], M. Grande [d], C.J. Howe [a], V.A. Fernandes [e,f], O. Gasnault [g], D.J. Lawrence [h], S.S. Russell [c], M.A. Wieczorek [i], B.H. Foing [j], The SMART-1 team

[a] Space Science and Technology Department, Rutherford Appleton Laboratory, Didcot, Oxon, OX11 0QX, UK
[b] UCL/Birkbeck Research School of Earth Sciences, UCL, Gower Street, London, WC1E 6BT, UK
[c] IARC, The Department of Mineralogy, The Natural History Museum, Cromwell Road, London SW7 5BD, UK
[d] Institute of Mathematical and Physical Sciences, University of Wales, Aberystwyth, Ceredigion, SY23 3BZ, UK
[e] Isotope Geochemistry and Cosmochemistry Group, SEAES, University of Manchester, Oxford Road Manchester, M13 9PL, UK
[f] Berkeley Geochronology Center, Berkeley, USA
[g] Centre d'Etude Spatiale des Rayonnements, CNRS/UPS, Toulouse, France
[h] Johns Hopkins University, Applied Physics Laboratory, Laurel, MD, USA
[i] Institut de Physique du Globe de Paris, France
[j] ESA Research and Scientific Support Department, ESTEC/SCI-S, Postbus 299, NL-2200 AG Noordwijk, The Netherlands

ARTICLE INFO

Article history:
Received 4 September 2008
Received in revised form
10 December 2008
Accepted 25 January 2009
Available online 1 February 2009

Keywords:
XRF spectroscopy
Moon
Space missions
Lunar science

ABSTRACT

The demonstration of a compact imaging X-ray spectrometer (D-CIXS), which flew on ESA's SMART-1 mission to the Moon (Racca et al., 2001; Foing et al., 2006), was designed to test innovative new technologies for orbital X-ray fluorescence spectroscopy. D-CIXS conducted observations of the lunar surface from January 2005 until SMART-1 impacted the Moon in September 2006. Here, we present scientific observations made during two solar flare events and show the first detection of Titanium Kα from the lunar surface. We discuss the geological implications of these results. We also discuss how experience from D-CIXS has aided the design of a similar instrument (Chandrayaan-1 X-ray Spectrometer (C1XS)) that was launched on the 22nd October 2008 on India's Chandrayaan-1 mission to the Moon.

1. Introduction

Global geochemical information is a requirement for understanding the complex compositional makeup of differentiated planetary bodies like the Moon. Theories of lunar evolution derived from petrological investigations of the Apollo and Luna samples have been greatly refined by the global elemental and mineralogical datasets provided by the Apollo X-ray fluorescence (XRF) and Gamma-ray experiments (Adler et al., 1973; Adler and Trombka, 1977; Andre et al., 1977), the Clementine (Lucey et al., 1998, 2000; Lucey, 2004; Pieters et al., 2006) and Lunar Prospector (Lawrence et al., 2002, 2003; Prettyman et al., 2006) missions, combined with studies of lunar meteorites. The Moon can no longer be thought of as simply being comprised of feldspathic highland (primary crust) and mare basalt (secondary crust) lithologies. Instead several different geochemically defined terranes have been identified (Clark and Hawke, 1981, 1991; Jolliff et al., 2000), necessitating a re-examination of lunar geological history (Wieczorek et al., 2006; Shearer et al., 2006). However, the global perspective is by no means complete yet, and new lunar orbital mapping missions are providing better spatially resolved data sets and the distribution of previously unmapped elements, helping to complete the global view of lunar crustal compositional heterogeneity.

X-ray spectroscopy is a powerful method for studying the major element concentration of geological materials. In a laboratory environment, a stabilised, and well characterised, X-ray or electron beam is used to provide the necessary energy for excitation of X-ray emission. In the case of an X-ray stimulus, the technique is referred to as X-ray fluorescence (XRF) spectroscopy. In planetary XRF studies, solar X-rays are the prerequisite exciting source (Yin et al., 1993), and typical levels of solar intensity will result in the excitation of low atomic number elements, including Mg, Al and Si. In periods of more intense activity (i.e. solar flares), excitation of heavier elements like P, K, Ca, Ti, Mn, Fe and Co can also occur (Yin et al., 1993). The technique can therefore be employed to study a range of different planetary inner solar system bodies like the Moon, Mercury and

* Corresponding author. Tel.: +44 0 1235 446271; fax: +44 0 1235 446667.
E-mail address: B.M.Swinyard@rl.ac.uk (B.M. Swinyard).

0032-0633/$ - see front matter © 2009 Elsevier Ltd. All rights reserved.
doi:10.1016/j.pss.2009.01.009

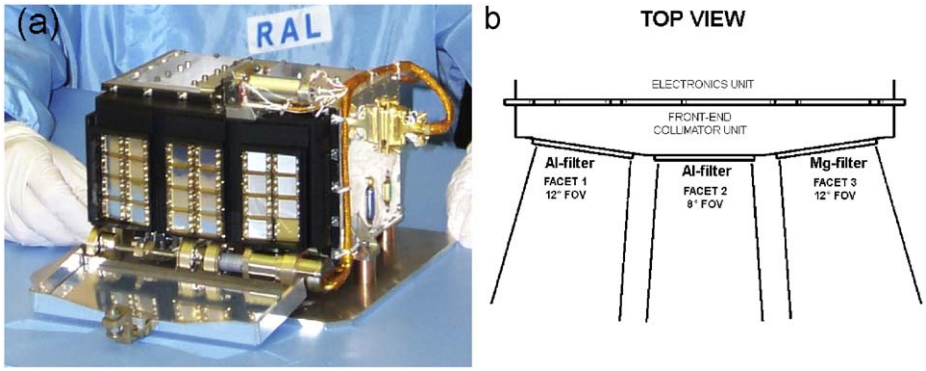

Fig. 1. (a) Photograph of the D-CIXS flight model (Image: RAL). (b) Schematic diagram of the D-CIXS front end assembly where—the view is shown looking down from the top of the instrument. The three Facet orientations are illustrated with their different opening angles and filter types.

asteroids (Adler et al., 1973; Adler and Trombka, 1977; Clark and Trombka, 1997a; Nittler et al., 2001; Grande et al., 2001, 2003; Okada et al., 2006; Schlemm et al., 2007; Okada et al., 2008; Fraser et al., Forthcoming), where there are no atmospheres to absorb the low energy incident and fluorescent X-rays, and where the solar flux is sufficiently high (Yin et al., 1993). XRF spectroscopy was first successfully demonstrated on the Moon by the Russian Luna 12 mission in 1968 (Mandel'Shtam et al., 1968), and the 1971 Apollo 15 and the 1972 Apollo 16 missions carried simple proportional counter experiments (Adler et al., 1972a, 1972b), measuring the X-ray photon count-rate from a limited area of the lunar surface (Adler et al., 1973). These data sets provided an initial understanding of the variable geochemistry of the lunar surface, paving the way for a new generation of lunar X-ray spectrometers. Note that the incident solar X-rays only penetrate into the upper few microns of a planetary surface, typically producing fluorescent X-rays from the outer layers of individual mineral grains (Clark and Trombka, 1997b).

The D-CIXS instrument (Fig. 1a, Grande et al., 2003; Dunkin et al., 2003) demonstrated a new approach to building miniaturized X-ray detectors, based around the use of innovative swept charge device (SCD) solid-state detectors (Holland et al., 2004). D-CIXS used 24 SCD detectors mounted in three facets consisting of eight detectors each. In an attempt to cover as much of the lunar surface as possible, these facets pointed in different directions—the central facet (Facet 2) pointed towards the spacecraft nadir, while adjacent facets (1 and 3) were angled by $\pm 10^\circ$ with respect to this (Fig. 1b). Each detector was equipped with a collimator giving a field of view of 8° for the central facet and 12° for the other two. Each collimator assembly on Facet 1 and 2 included two Al-filters (each 0.2 μm thick) to prevent light and low energy electrons from interacting with the SCDs. Facet 3 was also covered with a Mg filter, making these detectors relatively more sensitive to Mg fluorescence at low energy as the Al line is blocked (transmission at 1.49 keV is ~1/20 that of Mg) and the Si line is also very attenuated (transmission at 1.74 keV is ~1/4 that of Mg); mapping the distribution of Mg on the lunar surface was a high scientific priority for D-CIXS (Dunkin et al., 2003). D-CIXS was accompanied by an X-ray solar monitor (XSM) designed to monitor the solar input X-ray flux (Huovelin et al., 2002).

While successfully demonstrating the technology, the scientific results from D-CIXS (Grande et al., 2007) were limited by (i) the large and variable lunar footprint resulting from SMART-1's high, elliptical orbit (~300 × ~3000 km); (ii) radiation damage to the detectors during the long (15 month) journey to the Moon through the Earth's energetically charged particle belts; and (iii) unanticipated instrument and pre- and post-launch calibration problems (Grande et al., 2007). In addition to these operational constraints, D-CIXS orbited the Moon during a period (2005–2006) of very low solar activity (approaching the 2007 solar minimum), which both limited the X-ray signal and restricted the surface coverage to localities that were over flown during flare events. Even during solar flares other issues could cause the data to be difficult to interpret for one or more of the following reasons: (a) the observation viewing geometry was poor (i.e. near the lunar terminator); (b) the SCDs were flooded by incoming particles (electrons, protons, etc.) from the Sun, swamping any lunar XRF signal; (c) the instrument was turned off due to spacecraft temperature issues; or (d) sporadic interference of the SCD data processing produced a 'double peaked' spectrum which was difficult to retrospectively deconvolve.

During the mission, it also became clear that some individual detectors performed much better than others; in particular detectors 0 and 6 on Facet 1 displayed the lowest noise and narrowest spectral response. All observations reported here are based on X-ray flux measured by these two detectors. Calibration of the instrument response versus energy was carried out in flight using the Crab nebula as a calibration standard (Grande et al., 2007). This observation was only possible on Facet 2 (with aluminium filters), but, as the general shape of the response was similar between the detectors on Facet 2 and Facet 1, this response curve is taken as the average calibration for Facet 1 as well; no in-flight response calibration was possible for Facet 3 and these data are not considered calibrated.

The entire D-CIXS dataset has now been examined and a set of flare events during the lunar science mission were selected for analysis based upon their having suitable data with strong low-energy (Mg, Al and Si) lines and a line feature at ~3.7 keV associated with the Ca Kα line (Grande et al., 2007). Observations on the following two dates are of primary interest, as they coincide with large flares (M-class or above: Table 1) and contain suitable data for initial science analysis.

2. Observations

2.1. 'Farside flare' on July 27th 2005

An M1 to M2 class flare occurred between 04:45 and 04:52 UT when SMART-1 was orbiting over the central portion of the lunar farside Feldspathic Highlands Terrane ('FHT'; Fig. 2, Table 1). This region of the Moon is thought to be dominated by ferroan anorthosite (FAN) lithologies, representing primary crust formed at ~4.5 Ga during lunar differentiation (Taylor, 1982; Taylor et al., 1991; Jolliff et al., 2000). The terrane is heavily cratered,

Table 1
Viewing geometry solar flare state for the observations discussed in the text.

Time (UT)	Altitude (km)	Latitude (deg.)	Longitude (deg.)	Solar incidence angle (°)	GOES (XL Band)	GOES (XS Band)	Flare state
Nearside flare (18th November 2005)							
00:25	1014	−15.83	−23.38	14.93	1.54E-06	7.73E-08	C2
00:26	1037	−14,03	−23.51	13.07	1.77E-06	1.09E-07	C2
00:27	1060	−12.22	−23.67	10.97	2.72E-06	2.45E-07	C2
00:28	1084	−10.39	−23.86	9.19	4.28E-06	5.50E-07	C4
00:29	1108	−8.54	−24.06	7.34	6.15E-06	9.62E-07	C6
00:30	1133	−6.67	−24.36	5.25	8.05E-06	1.38E-06	C8
00:31	1157	−4.78	−24.46	3.38	1.02E-05	1.91E-06	M1
00:32	1182	−2.86	−24.65	1.94	1.19E-05	2.28E-06	M1
Farside flare (27th July 2005)							
04:45	1373	37.88	−136.93	70.33	1.05E-05	1.71E-06	M1
04:46	1344	36.33	−137.10	70.19	1.26E-05	2.11E-06	M1
04:47	1316	34.75	−137.27	70.04	2.47E-05	2.50E-06	M1
04:48	1287	33.15	−137.42	69.89	1.65E-05	2.90E-06	M2
04:49	1259	31.52	−137.57	69.61	1.85E-05	3.30E-06	M2
04:50	1230	29.86	−137.71	69.33	2.06E-05	3.67E-06	M2
04:51	1202	28.17	−137.85	69.04	2.25E-05	4.02E-06	M2
04:52	1173	26.45	−137.98	68.76	2.43E-05	4.63E-06	M2

Lunar coordinates and altitudes are given for the centre of Facet 1. The solar incidence angle is measured with respect to the surface normal. GOES XL (4.5 Å) and XS (1.75 Å) band fluxes are measured in $W\,m^{-2}$.

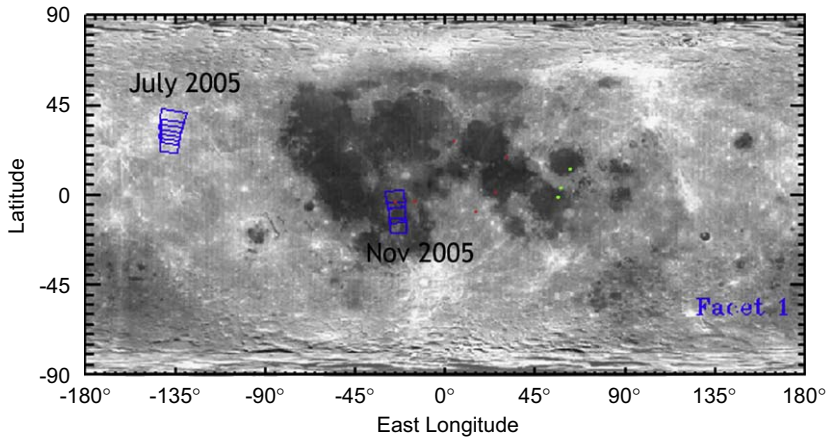

Fig. 2. Surface footprints of D-CIXS during the 'farside' (July 2005) and 'nearside' (November 2005) flare events discussed in this paper. Latitudes and Longitudes are provided in Table 1. Red points illustrate Apollo landing sites on the near-side of the Moon, and green points indicate the locality of the Luna sample return landing sites on the near-side Eastern limb. (For interpretation of the references to colour in this figure legend, the reader is referred to the web version of this article.)

but low-Fe concentrations (generally <7 wt% FeO) measured by Lunar Prospector (Lawrence et al., 2003) indicate that these impacts did not excavate mafic lower crustal rocks; modelling (Wieczorek et al., 2006) indicates a crustal thickness of 60–100 km in this region.

The X-ray spectrum for this flare is shown in Fig. 3 as the combined time-averaged spectra from detectors 0 and 6 on Facet 1. To determine the nature of the material giving rise to this spectrum, we have employed a forward modelling technique based on the method discussed in Clark and Trombka (1997b); further details of our modelling methods will be provided elsewhere (Swinyard et al., in preparation). The modeling requires knowledge of the incident solar spectrum from the flare (Clark and Adler, 1978; Clark and Trombka, 1997b). During the period of the flares, the XSM was not operational due to count rate saturation from the solar X-ray flux. Instead, we use X-ray flux data from the Geostationary Operational Environment Satellites (GOES: http://sxi.ngdc.noaa.gov/) for the period of the observation. From the GOES data, a flare temperature and brightness was derived that was used to construct a featureless spectrum based on the method described in Mewe et al. (1985). During the period of the observation, the flare temperature only varied by 10%, and although the overall intensity increased significantly, the normalisation procedure described below accounted for this: we therefore used the flare conditions at the end of the observation period, 00:52 UT, as representative of those prevalent during the entire observation. The model flare spectrum, together with the knowledge of the solar aspect angle (Table 1), was used to derive both the line flux and the Thomson-scattered X-ray flux. We have used a featureless spectrum as the absence of spectral information from the XSM, makes estimation of the line contribution difficult to assess. The only significant flare feature that is likely to impact on the model results is the Fe complex around 6.7 keV. Reuven Ramaty High Energy Solar Spectroscopic Imager (RHESSI) observations and comparisons to model predictions show that although the line intensity can vary considerably over the duration of a flare, the line to continuum for this line from flares in the $10–20\times10^6$ K temperature range, typical for an M-class

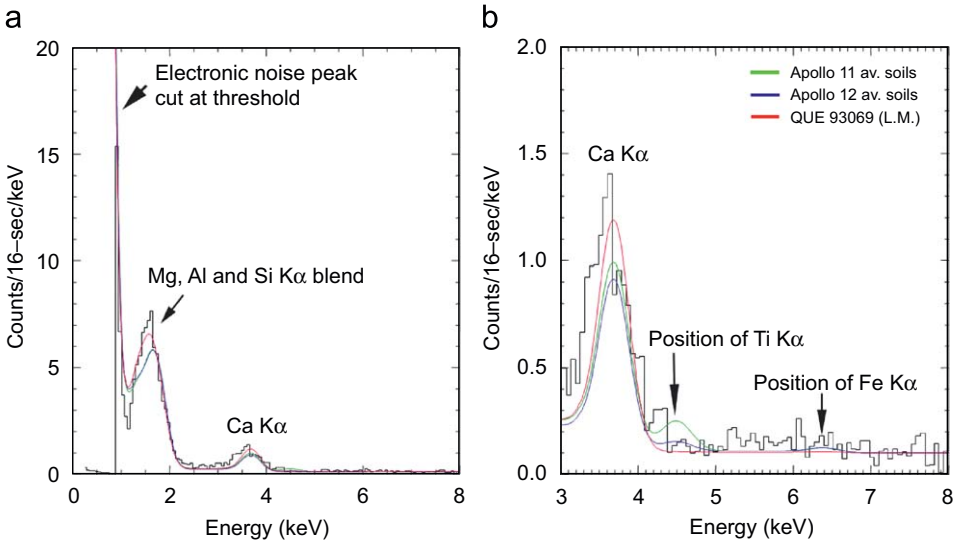

Fig. 3. Co-added spectra from detector 0 and detector 6 from the 27th July farside flare event (2005-07-27, UT 04:45 to 04:54) overlain with model predictions based on the composition of Apollo 11 (green), Apollo 12 (blue) soils and the feldspathic lunar meteorite (L.M.) QUE 93069 (red). (a) Full spectrum from 0 to 8 keV. (b) Scaled close-up of measured X-ray flux and models from 3 to 8 keV, illustrating the Ca Kα peak (3.7 keV). Note that, as expected for the farside, the model using lunar meteorite QUE 93069 gives the best agreement; the compositions adopted for the models are listed in Table 2. (For interpretation of the references to colour in this figure legend, the reader is referred to the web version of this article.)

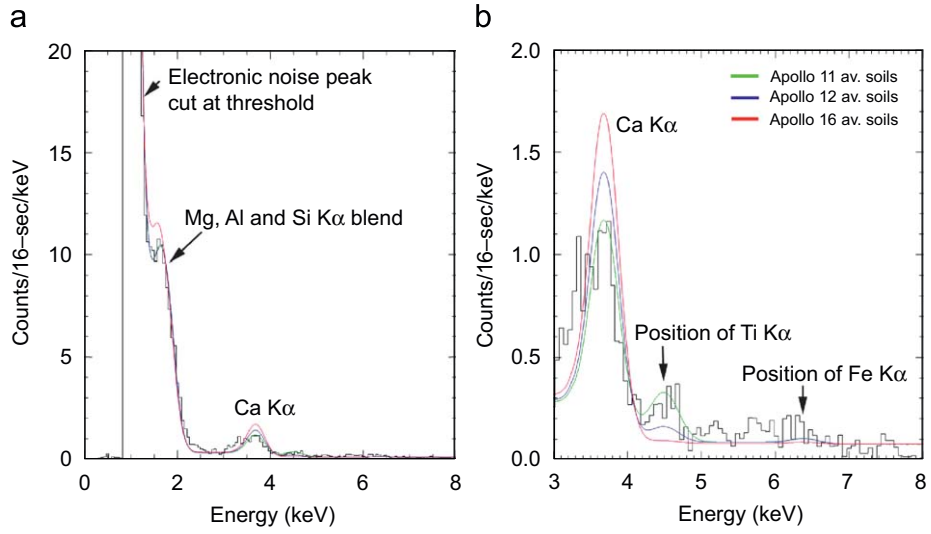

Fig. 4. Co-added spectra from detector 0 and detector 6 from the 18th November near-side flare event (2005-11-18, UT 00:28 to 00:32) overlain with model predictions of Apollo 11 (green), Apollo 12 (blue) and Apollo 16 (red) average soil compositions (Table 2). (a) Full spectrum from 0 to 8 keV. (b) Linear scaled close up of measured X-ray flux and models from 3 to 8 keV, illustrating the fit to the Ca Kα peak (3.7 keV) and a Ti Kα peak (4.5 keV). Note that the Ti concentration is intermediate between the Apollo 11 and Apollo 12 compositions; a least-variance fit to the data yields a Ti abundance of 3 ± 2 wt% (see text for details). (For interpretation of the references to colour in this figure legend, the reader is referred to the web version of this article.)

flare is never more than 10:1 (Phillips et al., 2006). Adding a line with intensity of 10 times the local continuum at the location of the Fe Kα, had no significant impact on the results for the predicted lunar fluorescence spectrum, showing that the approximation of using a featureless spectrum appears valid.

The model scattered solar continuum and fluorescent line fluxes were co-added, multiplied by the detector response versus energy derived from the Crab nebula, and convolved with an instrument spectral response function. This consisted of a 420 eV full width at half maximum (FWHM) Gaussian portion centred on the line energies plus a pedestal section corresponding to charge collection efficiency loss characteristic of the SCDs. The proportion of Gaussian to pedestal counts varies as a function of energy between 0.5 (at Mg, Al and Si) to ~0.2 at Fe. A noise peak is added at low energies with the position and height varied to fit the noise tail in the data and an overall fixed particle background is added to make the model coincide with the data at energies >10 keV. The latter was always between 0.05 and 0.1 counts/channel in 16 s integrations. Finally the model X-ray and noise spectrum, before addition of the particle background, was normalised to the data at the location of the Si Kα line at 1.74 keV. This process was carried out iteratively to ensure the noise peak in the model spectrum, matched the data. The apparent mismatch between the data and the model for the red (Apollo 16 type—see below) curve in Fig. 4 is due to the difference in magnesium concentration, not to a difference in the normalisation procedure. The same difference can be seen in Fig. 3, where the Apollo 16 model fits the data rather better than 11 or 12, but the noise peak for this spectrum was at a lower effective energy causing less interference with the fitting procedure.

Table 2
Geological compositions (elemental wt%) used for the X-ray modelling shown in Figs. 3 and 4.

Element wt%	Average bulk soils			Lunar meteorite
	Apollo 11	Apollo 12	Apollo 16	QUE 93069
Si	19.63	21.60	20.98	20.90
Ti	4.76	1.57	0.32	0.17
Al	6.66	6.42	14.41	15.50
Fe	12.75	13.36	3.87	3.24
Mg	4.78	6.28	3.62	2.70
Ca	8.39	7.04	10.41	11.80
Na	0.17	0.15	0.17	0.24
O	41.91	42.40	44.88	45.22
Total	99.05	98.82	98.66	99.77

The Apollo compositions are taken from bulk average landing site soil compositions as listed by Haskin and Warren (1991). Lunar meteorite QUE 93069 was selected as a best match to the composition of the lunar far side Feldspathic Highlands Terrane, and its bulk element bulk composition was taken from Warren et al. (2005).

The modelled line flux data were generated using the average composition (in elemental weight % concentrations) of Apollo landing site soils and lunar meteorites (Table 2, see also Korotev, 2005). The results of the model for Apollo 11 and Apollo 12 soils and a feldspathic lunar meteorite (QUE 93069; bulk composition taken from Warren et al., 2005) are overlaid on the data in Fig. 3. Whilst deriving concentration ratios is hampered by the poor spectral resolution of the instrument, these models indicate that a surficial regolith composition rich in aluminium and calcium (i.e. similar to lunar FAN meteorite QUE 93069) is required to best match the profile of the blended low-energy lines and the Ca Kα peak. The non-detection of Ti and Fe (Fig. 3b) in these data is also consistent with the expected Al-rich, Fe-poor, Ti-poor nature of the FHT inferred from interpretations of other remote sensing missions (Jolliff et al., 2000; Lucey et al., 2000; Prettyman et al., 2006).

2.2. 'Nearside flare' on the November 18th, 2005

The observations were made during a C2 to M1 class flare between 00:25 and 00:32 UT, when SMART-1 was over-flying the southern–central portion of the lunar near-side (Fig. 2, Table 1). The Facet 1 footprint included a mixed highlands-mare region south of and through Mare Cognitum, and over the Apollo 12 landing site area (Fig. 2). The co-added X-ray spectrum for this whole flare period, as measured by detectors 0 and 6, is shown in Fig. 4. Again, we have overlaid model spectra using the same method as described above and using the relevant viewing geometries and solar conditions listed in Table 1; the illustrated input model compositions used are average Apollo 11, 12 and 16 soils (Table 2). The flare temperature and intensity varied over the period of the observation. We elected to take the midpoint of the flare at 00:29 UT as representative of the average conditions during the observation (C6 class flare conditions: Table 1).

The low-energy lines (Mg, Al and Si) are best matched by models (Fig. 4a) with similar amounts of Mg and Al to the Apollo 11 and 12 soils (where Mg/Al = 0.72 and 0.98, respectively; Table 2), rather than compositions that are poorer in Mg and richer in Al (like the Apollo 16 site soils, where Mg/Al = 0.25: Table 2). Moreover, the Ca Kα line flux (Fig. 4b) is most similar to models with lower Ca abundances (i.e. appropriate for mare soils), compared with regoliths dominated by feldspathic material (i.e. Apollo 16 FAN-rich compositions). Significantly, and reported here for the first time for lunar XRF observations, we have clearly observed a feature at 4.5 keV coincident with the Ti Kα line. The signal-to-noise at the centre of the feature is ~4. We have performed a minimised variance fit to this feature and found that detection is at a confidence level of >95% (i.e. there is only a 5% chance of 0% concentration being compatible with the measurement). There is some evidence of an excess at the location of the Fe Kα line, which is above the prediction of the model due to fluorescence from the lunar surface alone; however, the low count rate and the presence of a noise excess over the 5–7 keV range, both in this and the far side spectrum, means that no real statistical certainty can be associated to the feature. The noise excess is not understood but is most likely due to the penetrating background events. (We note that D-CIXS was able to detect an Fe-line feature in much higher solar M-class and low X-flare observations of Mare Crisium, as discussed in Grande et al., 2007).

The minimum variance D-CXS Ti concentration is found to be 3 ± 2 wt% Ti (5 ± 3 wt% TiO_2). For comparison, the average Ti concentration obtained by the Lunar Prospector gamma-ray instrument is 1.95 ± 0.42 Ti wt% (1 standard deviation based on averaging 5° per pixel data within the D-CIXS footprints using data from the Prettyman et al., 2006 dataset), while that derived from Clementine using the Lucey et al., 2000 algorithm, and converting TiO_2 to Ti concentrations was 2.5 ± 0.9 wt% Ti (1 standard deviation based on averaging Clementine 1° per pixel data within the D-CIXS observation footprints). The D-CIXS value presented here is consistent with both these previous measurements and is similar to, although slightly higher than (probably as our field of view extends to mare regions beyond the landing site) the average Ti content (Table 2) of the Apollo 12 soils (1.57 ± 0.06 wt% Ti: Haskin and Warren, 1991).

3. Conclusions

This demonstration of a successful Ti concentration measurement is especially important given that Ti content is one of the primary diagnostics of mare basalt petrogenesis (Neal and Taylor, 1992). Although the Lunar Prospector and Clementine values are in good agreement in the region observed here; in general, significant discrepancies exist between these two data sets (e.g. Elphic et al., 2001) and XRF spectroscopy provides an independent means of determining the abundance of this important element. While, for the reasons outlined above, the spatial coverage and signal-to-noise ratio of the D-CIXS measurements are such that they cannot add significantly to the Clementine and Prospector results, they do augur well for the higher quality data expected from future instruments (see below).

Although the scientific results of D-CIXS were limited to favourable conditions, the instrument did fulfil its function as a technology demonstrator. Indeed, experience with D-CIXS has led to a significantly improved design for a similar instrument, the Chandrayaan-1 X-ray spectrometer (C1XS) that is now in orbit around the Moon onboard India's Chandrayaan-1 mission. C1XS will be a scientifically more powerful instrument than D-CIXS for several reasons (Crawford et al., 2009; Grande, 2009): (1) the short travel-time (c. 17 days) means that the detectors will be exposed to only 1% of the radiation damage that occurred in D-CIXS (based on laboratory calibrations, we anticipate an energy resolution of about 110 eV (at Al-Kα at <-20 °C) rather than 420 eV for the D-CIXS data presented here); (2) Chandrayaan-1's low circular orbit (100×100 km^2) will result in higher spatial resolution of the lunar surface (~25 km FWHM compared to 60–600 km for D-CIXS); (3) C1XS will operate during a more active period of the solar cycle, resulting in higher X-ray fluxes and greater sensitivity to compositional variations; and (4)

experience gained with D-CIXS has ensured that many of the instrumental and calibration problems have been eliminated from C1XS. Based on activity during previous cycles, we anticipate that more than 80% of the C1XS footprints will be illuminated at some time over a two-year mission by flare levels of C1 or above, permitting good detections of Mg, Al, Si, Ca, Ti and Fe (see Fig. 3 of Crawford et al., 2009). The latter two elements will be detectable, whenever its concentration in the surface is greater than about 1 wt% (as discussed in Section 3.5 of Crawford et al., 2009), facilitating the mapping and classification of mare basalt lava flows on a 25 km spatial scale. For these reasons, and largely building on the legacy of D-CIXS, we anticipate that C1XS will realise the full potential of lunar XRF spectroscopy and make significant contributions to lunar science.

Acknowledgements

We acknowledge the contributions of the entire D-CIXS team , the SMART-1 teams from ESA/ESTEC project, industrial teams, STOC Science and Technology Operations Centre and ESOC spacecraft operations, for their dedicated work in developing and navigating the spacecraft to reach the Moon and operation of the instruments. The D-CIXS instrument development was supported with SMART-1 funding from ESA Science and Technology Research Programmes, and funding sources (BNSC, RAL, PPARC/STFC). Additional hardware was provided by CESR, Toulouse, University of Helsinki observatory and IRF Kiruna, Sweden. We acknowledge exchange with instruments teams from SMART-1 Science and Technology Working Team (STWT). We also would like to thank the two anonymous reviewers, whose helpful comments improved the quality of this manuscript.

References

Adler, I., Trombka, J.I., 1977. Orbital chemistry—lunar surface analysis from the X-ray and gamma ray remote sensing experiments. Phys. Chem. Earth 10, 17.

Adler, I., Trombka, J., Gerard, J., Lowman, Schmadebeck, R., Blodget, H., Eller, E., Yin, L., Lamothe, R., Gorenstein, P., Bjorkholm, P., 1972a. Apollo 15 geochemical X-ray fluorescence experiment—preliminary report. Science 175, 436.

Adler, I., Trombka, J., Gerard, J., Lowman, P., Schmadebeck, R., Blodget, H., Eller, E., Yin, L., Lamothe, R., Osswald, G., Gorenstein, P., Bjorkholm, P., Gursky, H., Harris, B., 1972b. Apollo 16 geochemical X-ray fluorescence experiment—preliminary report. Science 177, 256.

Adler, I., Trombka, J.I., Lowman, P., Schmadebeck, R., Blodget, H., Eller, E., Yin, L., Lamothe, R., Osswakd, G., Gerard, J., Gorenstein, P., Bjorkhom, P., Gursky, H., Harris, B., Arnold, J., Metzer, A., Reedy, R., 1973. Apollo 15 and 16 results of the integrated geochemical experiment. The Moon 7, 487.

Andre, C.G., Bielefeld, M.J., Eliason, E., Soderblom, L.A., Adler, I., Philpotts, J.A., 1977. Lunar surface chemistry: a new imaging technique. Science 197, 986.

Clark, P.E., Hawke, B.R., 1981. Compositional variation in the Hadley Apennine region. Proc. Lunar Planet. Sci. Conf. 12th, 727.

Clark, P.E., Hawke, B.R., 1991. The lunar farside: the nature of the highlands east of Smythii. Earth, Moon Planets, 93 (appropriate for).

Clark, P.E., Trombka, J.I., 1997a. Remote X-ray fluorescence experiments for future missions to Mercury. Planet. Space Sci. 45, 57.

Clark, P.E., Trombka, J.I., 1997b. Remote X-ray spectrometry for NEAR and future missions: modeling and analyzing X-ray production from source to target. J. Geophys. Res. 102, 16631.

Clark, P.E., Adler, I., 1978. Utilization of independent solar flux measurements to eliminate nongeochemical variation in X-ray fluorescence data. Proc. Lunar Planet. Sci. Conf. 9th 3, 3029.

Crawford, I.A., Joy, K.H., Kellett, B.J., Grande, M., Anand, M., Bhandari, N., Cook, A.C., d'Uston, L., Fernandes, V.A, Gasnault, O., Goswami, J., Howe, C.J., Huovelin, J., Koschny, D., Lawrence, D.J., Maddison, B.J., Maurice,S., Narendranath, S., Pieters, C., Okada, T., Rothery, D.A., Russell, S.S., Sreekumar, P., Swinyard, B., Wieczorek, M., Wilding, M., 2009. The Scientific Rationale for the C1XS X-Ray Spectrometer on India's Chandrayaan-1 Mission to the Moon. Planet. Space Sci. (2009) in press, doi:10.1016/j.pss.2008.12.006.

Dunkin, S.K., Grande, M., Casanova, I., Fernandes, V., Heather, D.J., Kellett, B., Muinonen, K., Russell, S.S., Browning, R., Waltham, N., Parker, D., Kent, B., Perry, C.H., Swinyard, B., Perry, A., Feraday, J., Howe, C., Phillips, K., McBride, G., Huovelin, J., Muhli, P., Hakala, P.J., Vilhu, O., Thomas, N., Hughes, D., Alleyne, H., Grady, M., Lundin, R., Barabash, S., Baker, D., Clark, P.E., Murray, C.D., Guest, J., d'Uston, L.C., Maurice, S., Foing, B., Christou, A., Owen, C., Charles, P., Laukkanen, J., Koskinen, H., Kato, M., Sipila, K., Nenonen, S., Holmstrom, M., Bhandari, N., Elphic, R., Lawrence, D., 2003. Scientific rationale for the D-CIXS X-ray spectrometer on board ESA's SMART-1 mission to the Moon. Planet. Space Sci. 51, 435.

Elphic, R.C., Lawrence, D.J., Maurice, S., Feldman, W.C., Barraclough, B.L., Gasnault, O.M., Binder, A.B., Lucey, P.G., Blewett, D.T., 2001. Lunar Prospector neutron measurements and lunar TiO_2. Lunar Planet. Sci. Conf. XXXII Abstract #1487.

Foing, B.H., Racca, G.D., Marini, A., Evrard, E., Stagnaro, L., Almeida, M., Koschny, D., Frew, D., Zender, J., Heather, J., Grande, M., Huovelin, J., Keller, H.U., Nathues, A., Josset, J.L., Malkki, A., Schmidt, W., Noci, G., Birkl, R., Less, L., Sodnik, Z., McManamon, P., 2006. Adv. Space Res. 37, 6.

Fraser, G.W., Carpenter, J.D., Rothery, D.A., Pearson, J.F., Huovelin, J., Treis, J., Anttila, M., Ashcroft, M., Benkoff, J., Bowyer, A., Bradley, A., Bridges, J., Brown, C., Bulloch, C., Bunce, E.J., Christensen, U., Evans, M., Fairbend, R., Feasey, M., Giannini, F., Hermann, S., Hesse, M., Hilchenbach, M., Jorden, T., Joy, K., Kaipiainen, M., Kitchingman, I., Lechner, P., Lutz, G., Malkki, A., Martindale, A., Muinonen, K., Näränen, J., Portin, P., Prydderch, M., San Juan, J., Sclater, E., Schyns, E., Stevenson, T.J., Strüder, L., Syrjasuo, M., Talboys, D., Thomas, P., Whitford, C., Whitehead, S., forthcoming. The Mercury Imaging X-ray Spectrometer (MIXS) on BepiColombo. Planet. Space Sci., in revision.

Grande, M., Dunkin, S.K., Kellett, B., 2001. Opportunities for X-ray remote sensing at Mercury. Planet. Space Sci. 49, 1553.

Grande, M., Browning, R., Waltham, N., Parker, D., Dunkin, S.K., Kent, B., Kellett, B., Perry, C.H., Swinyard, B., Perry, A., Feraday, J., Howe, C., McBride, G., Phillips, K., Huovelin, J., Muhli, P., Hakala, P.J., Vilhu, O., Laukkanen, J., Thomas, N., Hughes, D., Alleyne, H., Grady, M., Lundin, R., Barabash, S., Baker, D., Clark, P.E., Murray, C.D., Guest, J., Casanova, I., D'Uston, L.C., Maurice, S., Foing, B., Heather, D.J., Fernandes, V., Muinonen, K., Russell, S.S., Christou, A., Owen, C., Charles, P., Koskinen, H., Kato, M., Sipila, K., Nenonen, S., Holmstrom, M., Bhandari, N., Elphic, R., Lawrence, D., 2003. The D-CIXS X-ray mapping spectrometer on SMART-1. Planet. Space Sci. 51, 427.

Grande, M., Kellett, B.J., Howe, C., Perry, C.H., Swinyard, B., Dunkin, S.K., Huovelin, J., Alha, L., D'Uston, L.C., Maurice, S., Gasnault, O., Couturier-Doux, S., Barabash, S., Joy, K.H., Crawford, I.A., Lawrence, D., Fernandes, V., Casanova, I., Wieczorek, M., Thomas, N., Mall, U., Foing, B., Hughes, D., Alleyne, H., Russell, S.S., Grady, M., Lundin, R., Baker, D., Murray, C.D., Guest, J., Christou, A., 2007. The D-CIXS X-ray spectrometer on the SMART-1 mission to the moon—first results. Planet. Space Sci. 55, 494.

Grande, M., Maddison, B.J., Howe, C.J., Kellett, B.J., Sreekumar, P., Huovelin, J., Crawford, I.A., Duston, C. L., Smith, D., Anand, M., Bhandari, N., Cook, A., Erd, C., Fernandes, V., Foing, B., Gasnaut, O, Goswami, J.N., Holland, A., Joy, K.H., Kochney, D., Lawrence, D., Maurice, S., Narendranath, S., Okada, T., Pieters, C., Rothery, D., Russell, S.S., Shrivastava, A., Swinyard, B.M., Wieczorek, M., Wilding, M., 2009. The C1XS X-ray spectrometer on Chandrayaan-1. Planet. Space Sci. (2009), in press, doi:10.1016/j.pss.2009.01.016.

Haskin, L., Warren, P., 1991. Lunar chemistry. In: Heiken, G.H., Vaniman, D., French, B.M. (Eds.), Lunar Sourcebook: A user's Guide to the Moon. Cambridge University Press, Cambridge, p. 357.

Holland, A.D., Hutchinson, I.B., Smith, D.R., Pool, P., 2004. Photon damage in the E2 V swept charge device. Nucl. Instrum. Methods Phys. Res. 521, 393.

Huovelin, J., Alha, L., Andersson, H., Andersson, T., Browning, R., Drummond, D., Foing, B., Grande, M., Hämäläinen, K., Laukkanen, J., Lämsä, V., Muinonen, K., Murray, M., Nenonen, S., Salminen, A., Sipilä, H., Taylor, I., Vilhu, O., Waltham, N., Lopez-Jorkama, M., 2002. The SMART-1 X-ray solar monitor (XSM): calibrations for D-CIXS and independent coronal science. Planet. Space Sci. 50, 1345.

Jolliff, B.L., Gillis, J.J., Haskin, L.A., Korotev, R.L., Wieczorek, M.A., 2000. Major lunar crustal terranes: surface expressions and crust-mantle origins. J. Geophys. Res. 105, 4197.

Korotev, R.L., 2005. Lunar geochemistry as told by lunar meteorites. Chem. Erde 65, 297.

Lawrence, D.J., Feldman, W.C., Elphic, R.C., Little, R.C., Prettyman, T.H., Maurice, S., Lucey, P.G., Binder, A.B., 2002. Iron abundances on the lunar surface as measured by the Lunar Prospector gamma-ray and neutron spectrometers. J. Geophys. Res. 107, 5130.

Lawrence, D.J., Elphic, R.C., Feldman, W.C., Prettyman, T.H., Gasnault, O., Maurice, S., 2003. Small-area thorium features on the lunar surface. J. Geophys. Res. 108, 5102.

Lucey, P.G., Blewett, D.T., Hawke, B.R., 1998. Mapping the FeO and TiO_2 content of the lunar surface with multispectral imagery. J. Geophys. Res. 103, 3679.

Lucey, P.G., Blewett, D.T., Jolliff, B.L., 2000. Lunar iron and titanium abundance algorithms based on final processing of Clementine ultraviolet-visible images. J. Geophys. Res. 105, 20297.

Lucey, P.G., 2004. Mineral maps of the moon. Geophys. Res. Lett. 3, L08701.

Mandel'Shtam, S.L., Tindo, I.P., Cheremukhin, G.S., Sorokin, L.S., Dmitriev, A.B., 1968. Lunar X-ray and the cosmic X-ray background measured by the lunar satellite LUNA-12. Cosmic Res. 6, 100.

Mewe, R., Gronenschild, E.H.B.M., van den Oord, G.H.J., 1985. Calculated X-radiation from optically thin plasmas V. Astron. Astrophys. Suppl. 62, 197.

Neal, C.R., Taylor, L.A., 1992. Petrogenesis of mare basalts: a record of lunar volcanism. Geochim. Cosmochim. Acta 56, 2177.

Nittler, L.R., Starr, R.D., Lim, L., McCoy, T.J., Burbine, T.H., Reedy, R.C., Trombka, J.I., Gorenstein, P., Squyres, S.W., Boynton, W.V., McClanahan, T.P., Bhangoo, J.S., Clark, P.E., Murphy, M.E., Killen, R., 2001. X-ray fluorescence measurements of the surface elemental composition of asteroid 433 Eros. Meteorit. Planet. Sci. 36, 1673.

Okada, T., Shirai, Kei, Yamamoto, Y., Arai, T., Ogawa, K.i., Hosono, K., Kato, M., 2006. X-ray fluorescence spectrometry of asteroid Itokawa by Hayabusa. Science 312, 1338.

Okada, T., Shirai, K., Yamamoto, Y., Arai, T., Ogawa, K., Shiraishi, H., Iwasaki, M., Kawamura, T., Morito, H., Kato, M., The SELENE XRS Team, 2008. X-ray fluorescence experiments on the SELENE (KAGUYA) spacecraft. 39th Annu. Lunar Planet. Sci. Conf. Abstract #1960.

Pieters, C., Shkuratov, Y., Kaydash, V., Stankevich, D., Taylor, L., 2006. Lunar soil characterization consortium analyses: pyroxene and maturity estimates derived from Clementine image data. Icarus 184, 83.

Phillips, K.J.H., Chifor, C., Dennis, B.R., 2006. RHESSI observations of the solar flare iron-line feature at 6.7 keV. Astrophys. J. 647, 1480.

Prettyman, T.H., Hagerty, J.J., Elphic, R.C., Feldman, W.C., Lawrence, D.J., McKinney, G.W., Vaniman, D.T., 2006. Elemental composition of the lunar surface: analysis of gamma-ray spectroscopy data from Lunar Prospector. J. Geophys. Res.—Planets 111, E12007.

Racca, G.D., Foing, B.H., Coradini, M., 2001. SMART-1: the first time of Europe to the moon. Earth, Moon Planets 85–86, 379.

Schlemm II, C.E., Starr, R.D., Ho, G.C., Bechtold, K.E., Benedict, S.A., Boldt, J.D., Boynton, W.V., Bradley, W., Fraeman, M.E., Gold, R.E., Goldsten, J.O., Hayes, J.R., Jaskulek, S.E., Rossano, E., Rumpf, R.A., Schaefer, E.D., Strohbehn, K., Shelton, R.G., Thompson, R.E., Trombka, J.I., Williams, B.D., 2007. The X-ray spectrometer on the MESSENGER spacecraft. Space Sci. Rev. 131, 393.

Shearer, C.K., Hess, P.C., Wieczorek, M.A., Pritchard, M.E., Parmentier, E.M., Borg, L., Longhi, J., Elkins-Tanton, L.T., Neal, C.R., Antonenko, I., Canup, R.M., Halliday, A.N., Grove, T.L., Hager, B.H., Less, D.-C., Wiechert, U., 2006. Thermal and magmatic evolution of the Moon. In: Jolliff, B.L., Wieczorek, M.A., Shearer, C.K., Neal, C.R. (Eds.), New Views Moon. Rev. Mineral. Geochem., vol. 60, p. 365.

Swinyard, B.M., et al., in preparation.

Taylor, G.J., Warren, P., Ryder, G., Delano, J., Pieters, C., Lofgren, G., 1991. Lunar rocks. In: Heiken, G., Vaniman, D., French, B. (Eds.), The Lunar Sourcebook: A User's Guide to the Moon. Cambridge University Press, Cambridge, p. 183 (Chapter 6).

Taylor, S.R., Planetary Science: A Lunar Perspective, 1982, Lunar Planet. Inst., Houston.

Warren, P.H., Ulff-Møller, F., Kallemeyn, G.W., 2005. "New" lunar meteorites: impact melt and regolith breccias and large-scale heterogeneities of the upper lunar crust. Meteorit. Planet. Sci. 40, 989.

Wieczorek, M.A., Jolliff, B.L., Khan, A., Pritchard, M.E., Weiss, B.P., Williams, J.G., Hood, L.L., Righter, K., Neal, C.R., Shearer, C.K., McCallum, I.S., Tompkins, S., Hawke, B.R., Peterson, C., Gillis, J.J., Bussey, B., 2006. The constitution and structure of the lunar interior. Rev. Mineral. Geochem. 60, 221.

Yin, L.I., Trombka, J.I., Adler, I., Bielefield, M., 1993. X-ray remote sensing techniques for geochemical analysis of planetary surfaces. In: Pieters, C.M., Englert, P.A. (Eds.), Remote Geochemical Analysis: Elemental and Mineralogical Composition. Cambridge University Press, Cambridge Website 〈http://sxi.ngdc.noaa.gov/〉 Last accessed 30th April 2008.